Ab initio calculation of the ion feature in x-ray Thomson scattering

Kai-Uwe Plagemann, Hannes R. Rüter, Thomas Bornath, Mohammed Shihab, Michael P. Desjarlais, Carsten Fortmann, Siegfried H. Glenzer, and Ronald Redmer

Ab initio calculation of the ion feature in x-ray Thomson scattering

Kai-Uwe Plagemann[1], Hannes R. Rüter[1], Thomas Bornath[1], Mohammed Shihab[1,2],
Michael P. Desjarlais[3], Carsten Fortmann[4], Siegfried H. Glenzer[5], and Ronald Redmer[1]

[1]*Institut für Physik, Universität Rostock, D-18051 Rostock, Germany*
[2]*Physics Department, Faculty of Science, Tanta University, 31527 Tanta, Egypt*
[3]*Sandia National Laboratories, Albuquerque, NM 87185, USA*
[4]*Quantumwise A/S, Lersø Parkallé 107, DK-2100 Copenhagen, Denmark*
[5]*High Energy Density Science, SLAC National Accelerator Laboratory, Menlo Park, CA 94025, USA*

The spectrum of x-ray Thomson scattering is proportional to the dynamic structure factor. An important contribution is the ion feature which describes elastic scattering of x-rays off electrons. We apply an *ab initio* method for the calculation of the form factor of bound electrons, the slope of the screening cloud of free electrons and the ion-ion structure factor in warm dense beryllium. With the presented method we can calculate the ion feature from first principles. These results will facilitate a better understanding of x-ray scattering in warm dense matter and an accurate measurement of ion temperatures which would allow determining non-equilibrium conditions, e.g., along shock propagation.

I. INTRODUCTION

X-ray Thomson scattering (XRTS) experiments [1–8] yield information on fundamental parameters such as electron and ion density, electron and ion temperature, and ionization state of high-density plasmas. Pump-probe experiments with variable time delay provide insight into the excitation and relaxation dynamics in dense plasmas on ultra-short time scales [4, 9]. Therefore, XRTS is considered as a key diagnostics in, e.g., compression experiments in order to obtain adequate results for the equation of state and further quantities such as the transport coefficients of warm dense matter (WDM). This is essential input data for interior and dynamo models of planets in the solar system and beyond [10, 11]. However, an accurate determination of these quantities is a great challenge, both for high-pressure experiments and many-particle theory.

The differential cross section for XRTS in the Born approximation is given by the total dynamic structure factor (DSF) of the electrons, $d^2\sigma/(d\omega d\Omega) = \sigma_T S_{ee}^{tot}(\vec{k},\omega)$, where $\hbar\vec{k}$ and $\hbar\omega$ are the transferred momentum and energy in the scattering process of x-rays at electrons, respectively. The Chihara formula [12] for the total DSF

$$S_{ee}^{tot}(\vec{k},\omega) = Z_f S_{ee}^0(\vec{k},\omega) + |f(\vec{k}) + q(\vec{k})|^2 S_{ii}(\vec{k},\omega)$$
$$+ Z_c \int_{-\infty}^{\infty} d\omega' \tilde{S}_{ce}(\vec{k},\omega') S_s(\vec{k},\omega - \omega') \quad (1)$$

is widely used for the evaluation of XRTS spectra [1, 2] and distinguishes contributions of free and bound electrons. The first term describes the DSF of free electrons with Z_f being the number of free electrons per nucleus. The second term gives the contribution of electrons following the ion motion and is usually referred to as the *ion feature*. Its amplitude is determined by the sum of the form factor $f(\vec{k})$ of bound electrons and the screening cloud $q(\vec{k})$ of free electrons. Although Chihara starts in his derivation from a division of the electrons into bound and free ones, at the end the ion feature is determined by total form factor $N(\vec{k}) = f(\vec{k}) + q(\vec{k})$. The ion-ion structure factor $S_{ii}(\vec{k},\omega)$ represents the thermal motion of the ions. The last term in Eq. (1) describes inelastic scattering of strongly bound (core) electrons due to Raman transitions to continuum states, $\tilde{S}_{ce}(\vec{k},\omega')$, which are modulated by the self-motion of ions, $S_s(\vec{k},\omega)$, and multiplied with the core charge Z_c.

To fully exploit the power of x-ray scattering measurements and to obtain reliable plasma parameters it is important to know precisely the important contributions in Eq. (1). For instance, the DSF of free electrons $S_{ee}^0(\vec{k},\omega)$ can be determined beyond the random phase approximation (RPA) by using the Mermin dielectric function [13] and considering electron-ion collisions in the Born approximation [1, 14–16]. The ion feature is of fundamental importance since it is a measure of the correlations of bound and free electrons and of the ion dynamics in WDM. It can be extracted from the XRTS spectrum [2] by weighting its contributions against the DSF of free electrons, the first term in Eq. (1), in conditions where bound-free transitions are well understood or negligibly small. However, several questions have to be addressed in this context, e.g., is a discrimination between free and bound electrons in WDM still feasible, what is the shape of the static and dynamic form factors, and what is the slope of the ion-ion structure factor, especially at low wavenumbers.

The ion feature has been studied by performing *ab initio* simulations for the static ion-ion structure factor $S_{ii}(\vec{k})$ [17, 18]. Its slope can be fitted via hypernetted chain calculations with respect to an effective potential that accounts for screening and, in addition, for short-range repulsion due to the bound electrons (HNC-SRR) [18, 19]. The form factor $f(\vec{k})$ and the screening

cloud $q(\vec{k})$ which enter the ion feature in Eq. (1) are usually calculated separately via approximate methods. This approach might be inadequate to address the above mentioned questions and, instead, a unified first-principles treatment of electrons and ions is chosen here.

Density functional theory molecular dynamics (DFT-MD) simulations for the ion feature of u-Be and CH were performed recently [20]. Applying the VASP package [21–23], ionic configurations where obtained. For beryllium, a two-valence-electrons pseudopotential was used; afterwards, static snapshots have been postprocessed in ABINIT [24] using a superhard pseudopotential accounting for all for electrons constituting beryllium.

In this study we calculate the ion feature solely from one first principles method using DFT-MD simulations which treat all four electrons per nucleus in the system on the same footing. In particular, we determine the static ion-ion and electron-ion (consisting of the form factor $f(\vec{k})$ and the screening cloud $q(\vec{k})$) structure factors for beryllium at conditions that have been probed in XRTS experiments: isochorically heated beryllium [14] (u-Be) at $\rho = 1.85$ g/cm^3 and a temperature of $T = 12$ eV, and shock-compressed beryllium [3] (c-Be) at $\rho = 5.5$ g/cm^3 and a temperature of $T = 13$ eV. Main goal of these experiments was to determine the parameters n_e and T_e using the inelastic scattering feature, additionally values for the ion feature were given.

The first-principles method to calculate the ion feature of beryllium is outlined in Sec. II, it can be applied to other materials such as carbon and aluminum as well. The results for the ion feature and the contributions of the ion-ion structure factor and of the form factor are presented in Sec. III. We compare with the XRTS data for u-Be and c-Be derived from laser-driven pump-probe experiments in Sec. IV and discuss the impact of non-equilibrium, two-temperature states. Conclusions can be found at the end of the paper.

II. THEORY

The dynamic structure factor $S_{\mathrm{ab}}(\vec{k}, \omega)$ can be calculated from the intermediate scattering function $F_{\mathrm{ab}}(\vec{k}, t)$ [25],

$$F_{\mathrm{ab}}(\vec{k}, t) = \frac{1}{\sqrt{N_a N_b}} \lim_{\tau \to \infty} \frac{1}{\tau} \int_0^\tau \rho_{\vec{k}}^a(t') \rho_{-\vec{k}}^b(t'+t) \mathrm{d}t', \quad (2)$$

$$S_{\mathrm{ab}}(\vec{k}, \omega) = \frac{1}{2\pi} \int_{-\infty}^\infty F_{\mathrm{ab}}(\vec{k}, t) e^{i\omega t} \mathrm{d}t, \quad (3)$$

with $\rho_{\vec{k}}^a(t)$ being the Fourier transformed particle density and N_a the number of particles of species a. Using DFT-MD runs the limit $\tau \to \infty$ extends to the duration of the simulation. If we assume that the nuclei are point-like particles located at positions $\vec{r}_v$, then $\rho_{\vec{k}}^i(t) = \sum_{v=1}^N e^{-i\vec{k}\cdot\vec{r}_v(t)}$.

The static structure factor results from the frequency integration of Eq. (3),

$$S_{\mathrm{ab}}(\vec{k}) = \int_{-\infty}^\infty S_{\mathrm{ab}}(\vec{k}, \omega) \mathrm{d}\omega = F_{\mathrm{ab}}(\vec{k}, t = 0). \quad (4)$$

This quantity contains the scattering pattern of the medium which reveals important structural information, e.g., the pair distribution functions $g_{ab}(\vec{r})$ by Fourier transformation,

$$S_{ab}(\vec{k}) = 1 + \sqrt{n_a n_b} \int (g_{ab}(\vec{r}) - 1) e^{i\vec{k}\cdot\vec{r}} \mathrm{d}\vec{r}. \quad (5)$$

We now focus on the second term in Eq. (1), the *ion feature*. The electron motion in this term is dominated by the ion dynamics, e.g. ion acoustic waves [26, 27], which are however not resolved in the considered experiments [3, 14]. Hence we can approximate the dynamic ion-ion structure factor as $S_{\mathrm{ii}}(\vec{k}, \omega) = S_{\mathrm{ii}}(\vec{k}) \delta(\omega)$, thereby introducing the static ion feature as

$$S_{\mathrm{ee}}^i(\vec{k}) = |f(\vec{k}) + q(\vec{k})|^2 S_{\mathrm{ii}}(\vec{k}) \equiv |N(\vec{k})|^2 S_{\mathrm{ii}}(\vec{k}). \quad (6)$$

The total form factor $N(\vec{k})$ is the Fourier transform of the mean electron charge distribution $N(\vec{r})$ around the nuclei. Anta and Louis [28] called this the density of a pseudo-atom. All pseudo-atom densities are superimposed according to the radial nucleus-nucleus radial distribution function $g_{ii}(\vec{r})$. This gives the total value of the electron density at $\vec{r}$

$$n_e g_{ei}(\vec{r}) = N(\vec{r}) + n_i \int \mathrm{d}\vec{r}' N(|\vec{r} - \vec{r}'|) g_{ii}(\vec{r}'). \quad (7)$$

Here, the electron-nucleus radial distribution function $g_{ei}(\vec{r})$ is the probability to find an electron, bound or free, at distance $\vec{r}$ from a nucleus at the origin. The electron density at $\vec{r}$ is therefore $n_e g_{ei}(\vec{r})$. Adopting the above relation (7), one neglects higher correlations of the nuclei as, e.g., molecules or other clustering. For the considered case of beryllium, this is undoubtedly justified.

For our calculations we use the finite temperature DFT-MD framework which combines classical molecular dynamics for the ions with a quantum treatment of the electrons based on DFT, see below. For given ion configurations, the electron density $\rho^e(\vec{r})$ is calculated from

$$\rho^e(\vec{r}) = \sum_n f_n |\phi_n(\vec{r})|^2, \quad (8)$$

with ϕ_n being the single electron wave functions and f_n the Fermi occupation numbers of states n with energy ϵ_n. In the same spirit as in Eq. (7), we write the electron density as a sum of a mean electron charge density $N(\vec{r})$ arround the different ions

$$\rho_e(\vec{r}, t) \approx \int \mathrm{d}\vec{r}' N(|\vec{r} - \vec{r}'|) \rho_i(\vec{r}', t), \quad (9)$$

or in Fourier space $\rho_{\vec{k}}^e(t) \approx N(\vec{k}) \rho_{\vec{k}}^i(t)$. The values $N(\vec{k})$ fluctuate slightly for the different time steps. Therefore the total form factor $N(\vec{k})$ is determined within this

ansatz by averaging over the time steps of the simulation,

$$N(\vec{k}) = \lim_{\tau \to \infty} \frac{1}{\tau} \int_0^\tau \frac{\rho_{\vec{k}}^e(t)}{\rho_{\vec{k}}^i(t)} \mathrm{d}t \,. \tag{10}$$

Thus we get for the fluid many-particle system an average pseudo-atomic form factor. From the definition of this quantity and accounting for charge neutrality, there follows that $N(k=0) = Z$.

In the case of warm dense beryllium, the valence and conduction band are separated by a huge energy gap which is found between -90 eV and -8 eV for u-Be and between -83 eV and -5 eV for c-Be. Notice that the free states can occupy weakly bound states due to the dynamics of the system so that they start slightly below zero. Therefore, we can distinguish between free (f) and bound (b) electron densities, $\rho^e(\vec{r}) = \rho_b^e(\vec{r}) + \rho_f^e(\vec{r})$, with

$$\rho_b^e(\vec{r}) = \sum_{\substack{n \\ \epsilon_n < \Delta}} f_n |\phi_n(\vec{r})|^2 \,, \ \rho_f^e(\vec{r}) = \sum_{\substack{n \\ \epsilon_n > \Delta}} f_n |\phi_n(\vec{r})|^2 \,. \tag{11}$$

We use a value of $\Delta = -40$ eV. The results are not sensitive with respect to a change of this parameter. By replacing $\rho_{\vec{k}}^e(t)$ in Eq. (10) with the Fourier transforms of $\rho_b^e(\vec{r})$ and $\rho_f^e(\vec{r})$, respectively, we get the bound electron form factor $f(\vec{k})$ for Be^{2+} ions and the screening cloud $q(\vec{k})$ of free electrons.

We want to emphasize that a separation of the total electron density into bound and free contributions is only possible if the energy gap is large enough as in the case of beryllium so that the precise choice of the parameter Δ has no influence on the results, as long as it separates the valence and conduction electrons. This might not be the case for other materials like carbon or aluminum where one has to calculate the ion feature, Eq. (6), via the total form factor $N(\vec{k})$, Eq. (10), in a strict physical picture using just the total electron density.

The finite temperature DFT-MD calculations were performed with the Vienna *ab initio* simulation package VASP 5.3. [21–23] using the provided projector augmented wave [29, 30] pseudopotential for the interaction between the nuclei and the electrons. We used the exchange-correlation (XC) functional of Perdew, Burke, and Ernzerhof [31]. Convergence was checked for particle numbers between 64 and 128 atoms and the energy cutoff for the plane wave expansion. The simulations were carried out with 64 Be atoms, each having four electrons, an energy cutoff of 1400 eV, and a simulation time of 5 ps up to 20 ps. The ion temperature was controlled with a Nosé thermostat [32]. Evaluations of the Brillouin zone were performed at the Baldereschi mean value point [33]. These parameters yield well-converged results, see [17].

III. RESULTS FOR THE ION FEATURE

One aim of XRTS experiments is to deliver information on the temperature of the system under investigation. In

order to show the influence of the temperature on the ion-ion structure factor and the total form factor, we performed DFT-MD simulations for u-Be [14] and c-Be [3] for various temperatures and evaluated the intermediate scattering function $F_{ab}(\vec{k}, t)$ according to Eq. (2). In the following we consider homogenous systems and therefore all quantities depend only on $|\vec{k}| = k$.

A. Static ion-ion structure factor

We calculate the ion-ion structure factor according to Eq. (4). Results are shown in Fig. 1 for u-Be and Fig. 2 for c-Be. Due to the finite simulation box, the structure factor cannot be determined for small wavenumbers k. Under the simulation conditions, the minimum value for k for 64 particles is ~ 1.1 Å^{-1}. Doubling the particle number yields a slightly smaller value of ~ 0.9 Å^{-1}, see Fig. 2 (black solid curve), but increases the numerical effort a lot. For numerical reasons we performed all calculations with 64 particles.

The structure factors at $k = 0$ can be calculated via an alternative way. In a charged particle system, the partial structure factors (electron-electron, ion-electron and ion-ion) are connected by $S_{ee}(k=0) = \sqrt{Z}S_{ei}(k=0) = ZS_{ii}(k=0)$ in the long-wavelength limit. Furthermore, the ion-ion structure factor is related to the isothermal compressibility κ_T by

$$S_{ii}(k=0) = n_i k_B T \kappa_T,$$
$$\kappa_T = -\frac{1}{V}\left(\frac{\partial V}{\partial p}\right)_T, \tag{12}$$

which is determined from corresponding equation of state data calculated via separate DFT-MD runs.
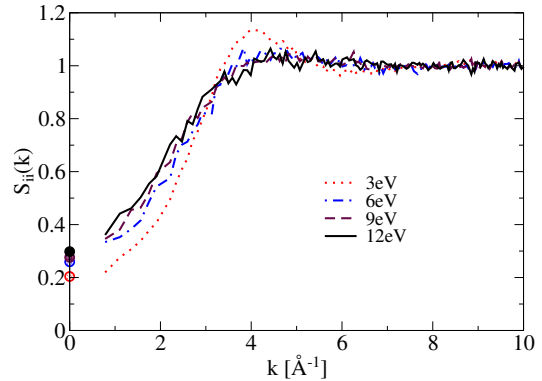

Figure 1. (Color online) Ion-ion structure factor for u-Be [14] for different temperatures. The circles at $k=0$ represent the values derived via the isothermal compressibility.

We have computed the ion-ion structure factor for temperatures of 12 eV (u-Be) [14] and 13 eV (c-Be) [3] as reported in the XRTS experiments, but also for additional temperatures of 3, 6, and 9 eV in order to study the impact of temperature. The results shown in Figs. 1 and
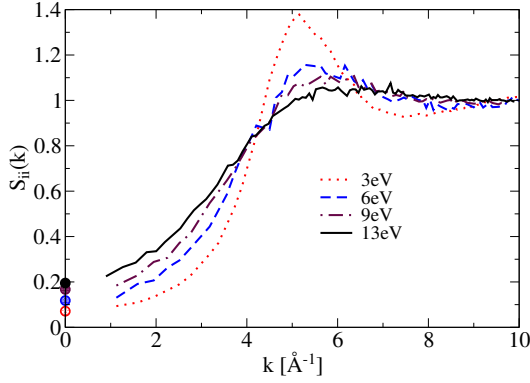
Figure 2. (Color online). Same as in Fig. 1 but for c-Be [3].

2 are in qualitative agreement with earlier DFT-MD results [17, 18]. For u-Be, Fig. 1, a very similar behavior is found for temperatures from 6 eV to 12 eV; only for 3 eV a slightly more pronounced structure results. Even for $k = 0$ only small differences occur, except for 3 eV. All curves represent a typical liquid-like behavior with correlations increasing towards the lowest temperature of 3 eV. For c-Be shown in Fig. 2 we observe more pronounced structures and a shift to higher k values due to stronger correlations between the particles for all temperatures. Again, the strongest correlation peak occurs for the lowest temperature of 3 eV.

B.   Form factor

Figure 3. (color online) Total form factor $N(k)$ (black), form factor of bound electrons $f(k)$ (red), and screening cloud of free electrons $q(k)$ (blue) for u-Be [14] at different temperatures. Red dash-dotted curve: Hartree-Fock form factor for Be^{2+} ions [34].

The total form factor N(k) is calculated from the DFT-MD simulations using directly the information contained in the Kohn-Sham wavefunctions. In order to compare with other approaches, we further calculated the contribution of the bound electrons, f(k), and the screening
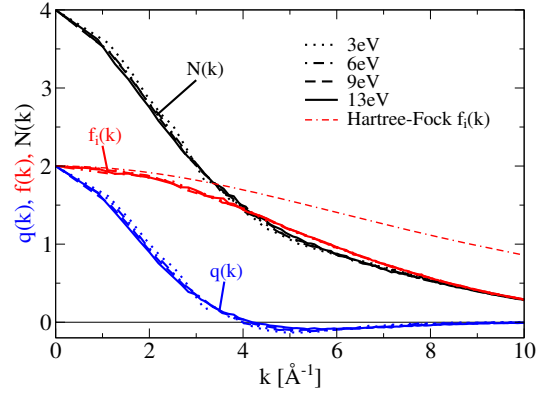
cloud q(k). As discussed above, this seems to be meaningful in the case of beryllium.

For the results shown in Figs. 3 and 4, the wavefunctions for several snapshots were evaluated and averaged. Only a weak dependence on temperature is observed. As expected, the form factor $f(k)$ and the screening cloud $q(k)$ converge to $f(k = 0) = q(k = 0) = 2$, i.e. beryllium consists of Be^{2+} ions and two unbound electrons per ion under these conditions. Inspection of Figs. 3 and 4 shows that for u-Be the screening cloud $q(k)$ becomes negative starting at values $k \approx 3.7$ Å^{-1} which indicates anti-screening [35] while for c-Be this behavior starts at $k \approx 4.1$ Å^{-1}. In the latter case the minimum is more pronounced and shifted due to compression. We compare also with the Hartree-Fock form factor [34] for Be^{2+} ions which exhibits increasing deviation from the *ab initio* results at larger wavenumbers and, thus, should not be used for WDM states.

C.   Ion feature

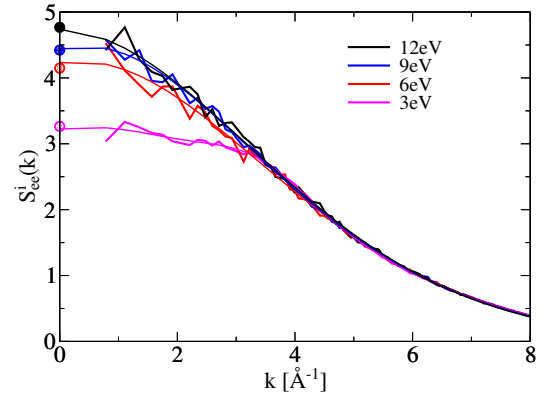Figure 4. (color online) Same as in Fig. 3 but for c-Be [3].

Figure 5. (color online) Ion feature for u-Be for different equilibrium temperatures. Thin lines are fits through the numerical data. The dots at $k = 0$ represent the values calculated from the isothermal compressibility.
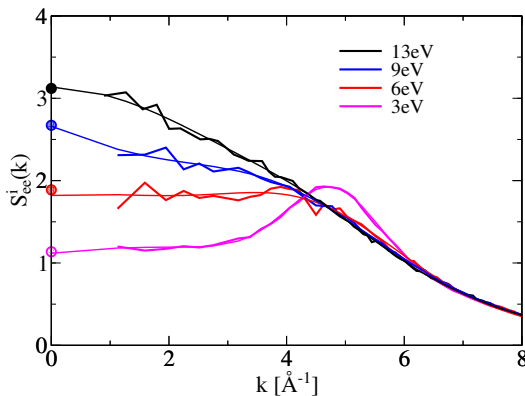
Figure 6. (color online) Same as in Fig. 5 but for c-Be.

We present the *ab initio* results for the temperature-dependent ion feature, Eq. (6), in Figs. 5 and 6 which are caluclated without any approximation for N(k) and $S_{ii}(\vec{k})$ other than the choice of the XC functional used in the DFT. In the long-wavelength limit the ion feature has the value $S_{ee}^i(k \to 0) = 16\,S_{ii}(k \to 0)$, thus it is mainly defined by the isothermal compressibility. In the investigated cases the ion feature for u-Be seems to decrease monotonically with increasing wavenumber for the considered parameters, and its temperature dependence is important only for $k < 3.5$ Å^{-1}. For c-Be the temperature dependence is stronger and visible for $k < 5$ Å^{-1}. Only for the lowest temperature of 3 eV does a pronounced maximum occur, which is at about $k = 5$ Å^{-1} due to the correlation peak in the ion-ion structure factor, see Fig. 2. For u-Be at a temperature of 12 eV, similar results for the ion feature were obtained in [20].

We conclude that our *ab initio* method for calculating the ion feature enables an accurate determination of the plasma parameters density and temperature because no approximation (except the choice of the XC functional used in the DFT calculations) has been made, neither for the form factors nor the ion-ion structure factor. The sensitivity is greatest for low k values. Since a measured spectrum contains all XRTS contributions, an accurate extraction of the elastic scattering contribution is required for diagnostic purposes. This problem is addressed in the next section.

IV. COMPARISON WITH XRTS EXPERIMENTS

A. Scattering spectrum and plasma parameters

Experimental values for the ion feature can be inferred in principle from measured XRTS spectra which represent the differential cross section on a relative scale. Provided that bound-free transitions can be neglected or their contribution is well defined, and that the elec-

tron feature (inelastic) and the ion feature (elastic) of the scattering signal can be well separated, the experimental values can be brought to an absolute scale using the f-sum rule

$$\int S_{ee}^0(k,\omega)\omega d\omega = \frac{\hbar^2 k^2}{2m_e}. \quad (13)$$

In practice, the electron feature of the signal is fitted, and a calibration constant C is determined from

$$\int I^{inelastic}(k,\omega)\omega d\omega = CZ_f\frac{\hbar^2 k^2}{2m_e}, \quad (14)$$

for Z_f we use here the values 2.105 for u-Be and 2.2 for c-Be, see [17]. Then, taking into account the instrumental function of the detector, $g(\omega)$, we have

$$I^{elastic}(k,\omega) = C \int S_{ee}^i(k)g(\omega - \omega')\delta(\omega')d\omega'$$
$$= CS_{ee}^i(k)g(\omega), \quad (15)$$

and get an experimental estimate for $S_{ee}^i(k)$. The instrumental function $g(\omega)$ is usually taken as a Gaussian.
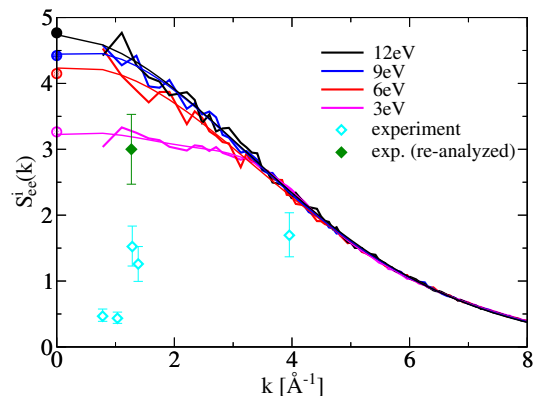

Figure 7. (color online) Ion feature for u-Be for different equilibrium temperatures. Thin lines are fits through the numerical data. The dots at $k = 0$ represent the values calculated from the isothermal compressibility. The dots with error bars represent experimental data (cyan) from Ref. [1] and a re-analyzed spectrum (green) given in Ref. [14].

The *ab initio* results for the ion feature are compared with data derived from XRTS spectra in Figs. 7 and 8. The values for the ion feature inferred in Refs. [1] and [3, 36] for u-Be and c-Be, respectively, from the experimental XRTS spectra (cyan dots with error bars) strongly deviate from the simulation results for low k values, while for medium values, $k \approx 4.5$ Å^{-1}, good agreement can be stated for both cases. For the medium k values we have $S_{ii}(k) \sim 1$ and $q(k) \sim 0$ so that the ion feature is determined by the bound electron form factor $f(k)$ alone, which shows for different temperatures only slight deviations, see Sec. III B.

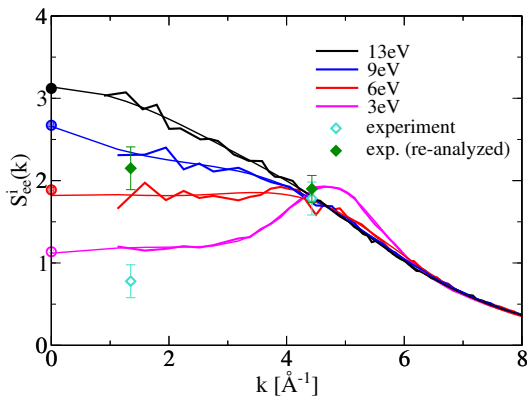The pronounced deviations between the *ab initio* results and the XRTS data at low k values have prompted

Figure 8. (color online) Same as in Fig. 7 but for c-Be. The dots with error bars represent experimental data (cyan) from [3, 36] and re-analyzed spectra (green).

Table I. Ion feature, calibration constant C (defined in Eq. (14)) and variance for the fits (a)-(c) shown in Fig. 9 for c-Be [3] at $k = 1.3$ Å^{-1} compared with the original value [3].

fit	C	ion feature	variance of the fit
(a)	5.46	2.15 ± 0.26	3.6×10^{-3}
(b)	8.42	1.20 ± 0.19	4.6×10^{-3}
(c)	11.28	0.75 ± 0.17	7.3×10^{-3}
[3]		0.78	7.2×10^{-3}

us to re-analyze experimental spectra available for u-Be [14] and c-Be [3, 36]. The spectra are relatively noisy. In the case of the compressed beryllium experiment, the analysis is even more difficult due to the double-peak structure of the x-ray photon source. The electron feature was fitted in this case by four Gaussians, while we used two Gaussians for u-Be.

We demonstrate the sensitivity of the fitting procedure in Fig. 9 where we show three acceptable fits (a)-(c) to the XRTS spectrum of c-Be at $k = 1.3$Å^{-1} (scattering angle 25°) [3, 36]. These fits lead to different calibration constants C, defined in Eq. (13) and given in Table I, and strongly different values for the ion feature, as well as the normalized variance of the fits.

Furthermore, we compare the best fit (a) (green), due to its slightest deviation, with the experimental XRTS spectrum [36] and the original fit (cyan) in Fig. 10. The re-analysis gives a better fit to the experimental spectrum (the variance is half of the value for the original fit) resulting in a better agreement with the theoretical prediction, see Fig. 7.

A re-analysis using the f-sum rule via Eq. (13) and Eq. (15) was performed for several available spectra for u-Be and c-Be. The results are shown as green symbols with error bars in Figs. 7 and 8. The corresponding ion features are shifted to higher values, being in much better agreement with the *ab initio* results.
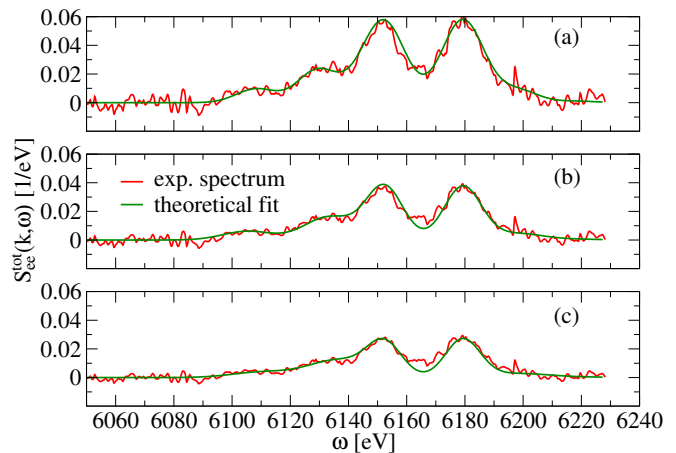

Figure 9. (color online) Different fits for the same experimental spectrum at $k = 1.3$Å^{-1} for c-Be [3] leading to different calibration constant C (Eq. (13)). Figure (a) shows the best fit to the scattering data, while (b) and (c) slightly different fits, but a strong derviation in the ion feature, see Table I.
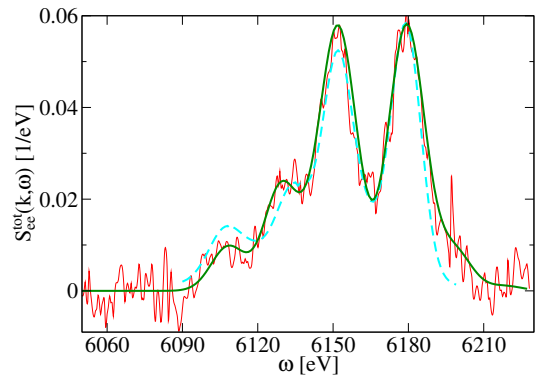

Figure 10. (color online) Normalized experimental scattering data for c-Be at $k = 1.3$ Å^{-1} (scattering angle 25°) in red, in cyan (dashed) the orignal fit [3] and in green (solid) our new fit (a).

B. Non-equilibrium effects

Although the re-analyzed data are shifted upwards towards the *ab initio* results (green dots with error bars in Figs. 7 and 8), they still do not agree with the curves for the temperatures, 12 eV and 13 eV, given in Refs. [1] and [3]. This requires certainly future experimental and theoretical investigations. For instance one could take into account possible non-equilibrium effects. Therefore, motivated by this discrepancy we performed additional DFT-MD simulations with different electron and ion temperatures [9, 37, 38], in order to study the effects of a non-equilibrium, two-temperature state that might have been created in these laser-driven experiments; see also [38, 39]. We assume electron temperatures as reported in the experiments (12 eV for u-Be and 13 eV for c-Be), but make calculations also for lower ion temperatures of 6 eV and 9 eV, see Figs. 11 and 12. There is
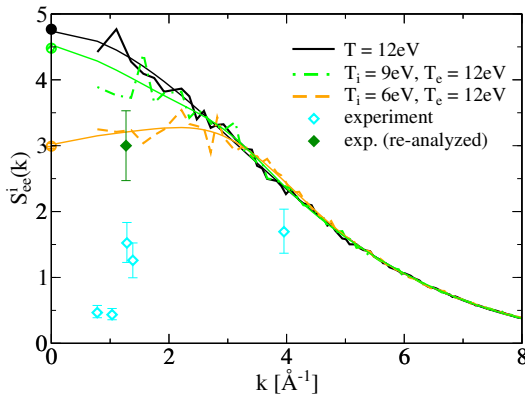
Figure 11. (color online) Ion feature for u-Be for non-equilibrium two-temperature systems. Thin lines are fits through the numerical data. The dots at $k = 0$ represent the values calculated from the isothermal compressibility. The dots with error bars represent experimental data (cyan) from Ref. [1] and a re-analyzed spectrum (green) given in Ref. [14].
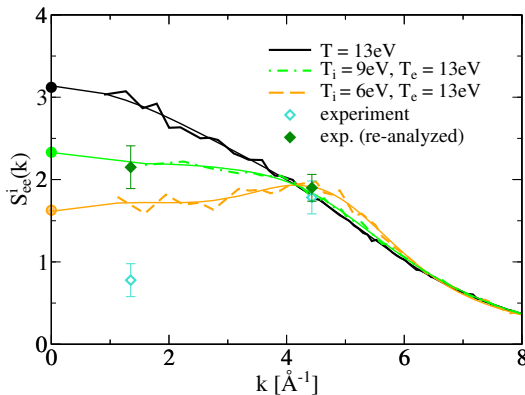

Figure 12. (color online) Same as in Fig. 11 but for c-Be. The dots with error bars represent experimental data (cyan) from [3, 36] and re-analyzed spectra (green).

a good agreement of the re-analyzed data with the *ab initio* simulations for an ion temperature of 6 eV (orange dashed) for u-Be and an ion temperature of 9 eV (green dash-dotted) for c-Be. Whether or not such two-temperature states were generated in the experimental setups should be addressed in future experiments.

V. CONCLUSION

In conclusion, we have determined the ion feature of warm dense beryllium from first principles. No input

for the form factor, the screening cloud, and the ion-ion structure factor was used; all quantities were determined self-consistently within the DFT-MD simulations. We observe for u-Be only a weak temperature dependence which is more pronounced for c-Be. The *ab initio* results for the form factor indicate that standard methods of atomic physics like Hartree-Fock have to be used with care for WDM. We find agreement with experimental data for the ion feature at medium k vectors in both cases while significant deviations occur for low k values. Re-analyzing the quite noisy spectra that were recorded in these first XRTS experiments [1, 3, 14, 36] by using the f-sum rule, considerably larger ion features were obtained in this range, in much better agreement with the *ab initio* results. In addition the data points indicate that a two-temperature state might have been created in the XRTS experiments, with lower ion temperatures of about 6 eV and 9 eV, respectively.

Novel XRTS experiments with a much better spectral resolution are necessary in order to verify the ion feature in warm dense matter, especially its low-k behavior, its temperature dependence and possible non-equilibrium effects. Such experiments could be performed at free electron laser facilities like LCLS using the seeded x-ray mode which would provide the required spectral resolution combined with a high peak brilliance, see [8]. In such future studies our new results will help to use the absolute intensity of the elastic scattering feature to measure the ion temperatures and to identify non-equilibrium conditions.

[1] S. H. Glenzer and R. Redmer, Rev. Mod. Phys. **81**, 1625 (2009).

[2] C. Fortmann, T. Bornath, R. Redmer, H. Reinholz, G. Röpke, V. Schwarz, and R. Thiele, Laser Part. Beams **27**, 311 (2009).

[3] H. J. Lee, P. Neumayer, J. Castor, T. Döppner, R. W. Falcone, C. Fortmann, B. A. Hammel, A. L. Kritcher, O. L. Landen, R. W. Lee, D. D. Meyerhofer, D. H. Munro, R. Redmer, S. P. Regan, S. Weber, and S. H. Glenzer, Phys. Rev. Lett. **102**, 115001 (2009).

[4] A. L. Kritcher, P. Neumayer, J. Castor, T. Doppner, R. W. Falcone, O. L. Landen, H. J. Lee, R. W. Lee, B. Holst, R. Redmer, E. C. Morse, A. Ng, S. Pollaine, D. Price, and S. H. Glenzer, Physics of Plasmas **16**, 056308 (2009).

[5] C. Fortmann, H. J. Lee, T. Döppner, R. W. Falcone, A. L. Kritcher, O. L. Landen, and S. H. Glenzer, Phys. Rev. Lett. **108**, 175006 (2012).

[6] S. White, G. Nersisyan, B. Kettle, T. Dzelzainis, K. Mc-Keever, C. Lewis, A. Otten, K. Siegenthaler, D. Kraus, M. Roth, T. White, G. Gregori, D. Gericke, R. Baggott, D. Chapman, K. Wünsch, J. Vorberger, and D. Riley, High Energy Dens. Phys. **9**, 573 (2013).

[7] D. Kraus, J. Vorberger, D. O. Gericke, V. Bagnoud, A. Blažević, W. Cayzac, A. Frank, G. Gregori, A. Ortner, A. Otten, F. Roth, G. Schaumann, D. Schumacher, K. Siegenthaler, F. Wagner, K. Wünsch, and M. Roth, Phys. Rev. Lett. **111**, 255501 (2013).

[8] L. B. Fletcher, H. J. Lee, T. Döppner, E. Galtier, B. Nagler, P. Heimann, C. Fortmann, S. LePape, T. Ma, M. Millot, A. Pak, D. Turnbull, D. A. Chapman, D. O. Gericke, J. Vorberger, T. White, G. Gregori, M. Wei, B. Barbrel, R. W. Falcone, C.-C. Kao, H. Nuhn, J. Welch, U. Zastrau, P. Neumayer, J. B. Hastings, and S. H. Glenzer, Nat. Photon. **9**, 274 (2015).

[9] U. Zastrau, P. Sperling, M. Harmand, A. Becker, T. Bornath, R. Bredow, S. Dziarzhytski, T. Fennel, L. B. Fletcher, E. Förster, S. Göde, G. Gregori, V. Hilbert, D. Hochhaus, B. Holst, T. Laarmann, H. J. Lee, T. Ma, J. P. Mithen, R. Mitzner, C. D. Murphy, M. Nakatsutsumi, P. Neumayer, A. Przystawik, S. Roling, M. Schulz, B. Siemer, S. Skruszewicz, J. Tiggesbäumker, S. Toleikis, T. Tschentscher, T. White, M. Wöstmann, H. Zacharias, T. Döppner, S. H. Glenzer, and R. Redmer, Phys. Rev. Lett. **112**, 105002 (2014).

[10] M. French, A. Becker, W. Lorenzen, N. Nettelmann, M. Bethkenhagen, J. Wicht, and R. Redmer, Astrophys. J. Suppl. **202**, 5 (2012).

[11] A. Becker, W. Lorenzen, J. Fortney, N. Nettelmann, M. Schöttler, and R. Redmer, Astrophys. J. Suppl. **215**, 21 (2014).

[12] J. Chihara, J. Phys. Cond. Matter **12**, 231 (2000).

[13] N. D. Mermin, Phys. Rev. B **1**, 2362 (1970).

[14] S. H. Glenzer, O. L. Landen, P. Neumayer, R. W. Lee, K. Widmann, S. W. Pollaine, R. J. Wallace, G. Gregori, A. Höll, T. Bornath, R. Thiele, V. Schwarz, W.-D. Kraeft, and R. Redmer, Phys. Rev. Lett. **98**, 065002 (2007).

[15] A. Höll, T. Bornath, L. Cao, T. Döppner, S. Düsterer, E. Förster, C. Fortmann, S. Glenzer, G. Gregori, T. Laarmann, K.-H. Meiwes-Broer, A. Przystawik, P. Radcliffe, R. Redmer, H. Reinholz, G. Röpke, R. Thiele, J. Tiggesbäumker, S. Toleikis, N. Truong, T. Tschentscher, I. Uschmann, and U. Zastrau, High Energy Dens. Phys. **3**, 120 (2007).

[16] C. Fortmann, A. Wierling, and G. Röpke, Phys. Rev. E **81**, 026405 (2010).

[17] K.-U. Plagemann, P. Sperling, R. Thiele, M. Desjarlais, C. Fortmann, T. Döppner, H. Lee, S. Glenzer, and R. Redmer, New J. Phys. **14**, 055020 (2012).

[18] K. Wünsch, J. Vorberger, and D. O. Gericke, Phys. Rev. E **79**, 010201(R) (2009).

[19] J. Vorberger and D. O. Gericke, High Energy Dens. Phys. **9**, 178 (2013).

[20] J. Vorberger and D. O. Gericke, Phys. Rev. E **91**, 033112 (2015).

[21] G. Kresse and J. Hafner, Phys. Rev. B **47**, 558 (1993).

[22] G. Kresse and J. Hafner, Phys. Rev. B **49**, 14251 (1994).

[23] G. Kresse and J. Furthmüller, Phys. Rev. B **54**, 11169 (1996).

[24] X. Gonze, B. Amadon, P.-M. Anglade, J.-M. Beuken, F. Bottin, P. Boulanger, F. Bruneval, D. Caliste, R. Caracas, M. Côté, T. Deutsch, L. Genovese, P. Ghosez, M. Giantomassi, S. Goedecker, D. Hamann, P. Hermet, F. Jollet, G. Jomard, S. Leroux, M. Mancini, S. Mazevet, M. Oliveira, G. Onida, Y. Pouillon, T. Rangel, G.-M. Rignanese, D. Sangalli, R. Shaltaf, M. Torrent, M. Verstraete, G. Zerah, and J. Zwanziger, Comput. Phys. Commun. **180**, 2582 (2009).

[25] L. van Hove, Phys. Rev. **95**, 249 (1954).

[26] T. G. White, S. Richardson, B. J. B. Crowley, L. K. Pattison, J. W. O. Harris, and G. Gregori, Phys. Rev. Lett. **111**, 175002 (2013).

[27] H. R. Rüter and R. Redmer, Phys. Rev. Lett. **112**, 145007 (2014).

[28] J. A. Anta and A. A. Louis, Phys. Rev. B **61**, 11400 (2000).

[29] P. E. Blöchl, Phys. Rev. B **50**, 17953 (1994).

[30] G. Kresse and D. Joubert, Phys. Rev. B **59**, 1758 (1999).

[31] J. P. Perdew, K. Burke, and M. Ernzerhof, Phys. Rev. Lett. **77**, 3865 (1996).

[32] S. Nosé, J. Chem. Phys. **81**, 511 (1984).

[33] A. Baldereschi, Phys. Rev. B **7**, 5212 (1973).

[34] E. Prince (ed.), *International Tables for Crystallography*, Vol. C (John Wiley & Sons, 2006) p. 566.

[35] D. O. Gericke, J. Vorberger, K. Wünsch, and G. Gregori, Phys. Rev. E **81**, 065401 (2010).

[36] H. J. Lee, T. Döppner, P. Neumayer, J. Castor, R. W. Falcone, C. Fortmann, B. A. Hammel, A. L. Kritcher, O. L. Landen, R. W. Lee, D. D. Meyerhofer, D. H. Munro, R. Redmer, S. P. Regan, S. Weber, R. Wallace, and S. H. Glenzer, Journal of Physics: Conference Series **244**, 042015 (2010).

[37] Z. Chen, B. Holst, S. E. Kirkwood, V. Sametoglu, M. Reid, Y. Y. Tsui, V. Recoules, and A. Ng, Phys. Rev. Lett. **110**, 135001 (2013).

[38] J. Clérouin, G. Robert, P. Arnault, C. Ticknor, J. D. Kress, and L. A. Collins, Phys. Rev. E **91**, 011101 (2015).

[39] D. A. Chapman and D. O. Gericke, Phys. Rev. Lett. **107**, 165004 (2011).